N65-88106
(ACCESSION NUMBER)
29
(PAGES)
(NASA CR OR TMX OR AD NUMBER)
(THRU)
None
(CODE)
(CATEGORY)
FACILITY FORM 602

62 62334
Copy 21
RM SL53I30a

NACA

RESEARCH MEMORANDUM

for the

Bureau of Aeronautics, Department of the Navy

DECLASSIFIED - EFFECTIVE 1-15-64
Authority: Memo Geo. Drobka NASA HQ.
Code ATSS-A Dtd. 3-12-64 Subj: Change
in Security Classification Marking.

RESULTS OF A POWER-ON FLIGHT OF A 1/10-SCALE ROCKET-PROPELLED MODEL OF THE CONVAIR XF2Y-1 AIRPLANE AT A MACH NUMBER OF 1.53

TED NO. NACA DE 365

By William M. Bland, Jr., and Robert L. Nelson

Langley Aeronautical Laboratory
Langley Field, Va.

Declassified by authority of NASA
Classification Change Notices No. 217-6
Dated ** 9/15/62

[redacted]

[redacted]

NATIONAL ADVISORY COMMITTEE
FOR AERONAUTICS
WASHINGTON
SEP 28 1953

[redacted]

DECL[redacted]IFIED

NATIONAL ADVISORY COMMITTEE FOR AERONAUTICS

RESEARCH MEMORANDUM

for the

Bureau of Aeronautics, Department of the Navy

DECLASSIFIED - EFFECTIVE 1-15-64
Authority: Memo Geo. Drobka NASA HQ.
Code ATSS-A Dtd. 3-12-64 Subj: Change
in Security Classification Marking.

RESULTS OF A POWER-ON FLIGHT OF A 1/10-SCALE ROCKET-PROPELLED MODEL OF THE CONVAIR XF2Y-1 AIRPLANE AT A MACH NUMBER OF 1.53

TED NO. NACA DE 365

By William M. Bland, Jr., and Robert L. Nelson

SUMMARY

A 1/10-scale model of the Convair XF2Y-1 airplane containing solid-fuel rocket motors designed to simulate the full-scale turbojet-engine characteristics at an altitude of 35,000 feet with full afterburning has been flight tested at a Mach number of 1.53. All results were obtained during power-on flight.

Results of this flight indicated that the model had dynamic lateral instability, but under conditions not likely to be encountered by the full-scale airplane. It was also shown that the pitching moment at zero lift was increased approximately 30 percent (nose down) by the low-pressure regions over the rear portion of the fuselage exposed to the jet. The lift-curve slope was approximately 25 percent lower than values obtained from wind-tunnel tests. The value obtained for the directional-stability parameter agreed with the value estimated by Convair for the full-scale flexible airplane. The minimum drag coefficient determined for this model, which had closed inlets, was approximately 25 percent greater than the value obtained from wind-tunnel tests of a model with open inlets, but with different aft fuselage geometry.

INTRODUCTION

At the request of the Bureau of Aeronautics, Department of the Navy, 1/10-scale models of the Convair XF2Y-1 airplane are being flight tested at

high subsonic, transonic, and supersonic speeds by the Langley Pilotless Aircraft Research Division to determine the minimum drag, some lateral and longitudinal stability characteristics, and the effect of jet exhaust over the body on trim. The Convair XF2Y-1, which is a twin-turbojet-engined tailless configuration with thin, low-aspect-ratio, modified delta wings and vertical surface, is designed to be a water-based supersonic fighter airplane.

This investigation, which is being conducted with rocket-propelled models in free flight, has been started with the flight test of one model at the Pilotless Aircraft Research Station, Wallops Island, Va. This model was flight tested primarily to determine the effect of jet exhaust over the rear portion of fuselage (hereafter referred to as beach area) on the airplane trim and to determine some longitudinal and lateral stability characteristics. The jet was provided by a solid-propellant rocket motor, contained within the model, that was designed to simulate jet-engine characteristics of the full-scale airplane at a Mach number of 1.5 at an altitude of 35,000 feet.

SYMBOLS

S	total included wing area, sq ft
$\bar{c}$	wing mean aerodynamic chord, ft
z	vertical distance between thrust line and center of gravity, ft
ϵ	angle between longitudinal principal axis and longitudinal body axis, positive when body axis is rotated above principal axis at the nose, deg
A	cross-sectional area of equivalent body
r_{equiv}	radius of equivalent body of revolution
D_{max}	maximum diameter of equivalent body
l	body length
X	distance from nose, in.
r	radius of curvature of beach in plane normal to longitudinal body axis, in.

φ_1, φ_2 limits of integration around surface of the beach at any station X, deg

K effective area on one beach at any station X on beach

M Mach number

R Reynolds number (based on $\bar{c}$)

q free-stream dynamic pressure, lb/sq ft

α angle of attack, deg

β angle of sideslip, deg

p_a atmospheric static pressure, lb/sq ft

p local static pressure, lb/sq ft

P pressure coefficient, $\frac{p - p_a}{q}$

C_N normal-force coefficient, $\frac{\text{Normal force}}{qS}$

C_Y side-force coefficient, $\frac{\text{Side force}}{qS}$

C_C chord-force coefficient, $\frac{\text{Chord force}}{qS}$

C_T thrust coefficient, $\frac{\text{Thrust}}{qS}$

$C_{L_\alpha} = \frac{\partial C_L}{\partial \alpha} \approx \frac{\partial C_N}{\partial \alpha}$

C_{m_α} longitudinal-stability parameter

C_m/C_L aerodynamic-center location with respect to leading edge of mean aerodynamic chord

$C_{m_q} + C_{m_{\dot{\alpha}}}$ damping-in-pitch coefficient

C_{n_β} directional-stability parameter

[redacted]

Subscripts:

o	zero lift
t	trim
min	minimum

MODEL DESCRIPTION

The general characteristics of the model are shown in the drawing in figure 1, in the photographs in figure 2, and in table I. The area distribution of the model and the profile of a body of revolution with an equivalent area distribution are shown in figure 3.

The wings were constructed of laminated wood with aluminum-alloy chord-plane stiffeners and inlays under the wing surface. The construction of the vertical tail was similar except that the aluminum-alloy inlays were omitted. The fuselage shell was made of plastic-fiberglass laminate. The elevons and rudder were not deflected.

The duct inlets on this model were closed with approximately spherical covers (fig. 2(a)) and the space alloted for ducting and turbojet engines in the full-scale airplane was used to house a solid-propellant rocket motor, as shown in figure 4(a). This solid-propellant rocket motor was designed to simulate the scale mass flow, exit pressure ratio, and thrust of the full-scale turbojet engines at $M = 1.5$ at an altitude of 35,000 feet with full afterburning.

Instruments and telemetering equipment were installed in the nose, above the wing ahead of the rocket motor, and below the wing as shown in the photographs in figure 4. The instruments, which were 14 in number, were used to measure angle of attack, accelerations along each body axis, total and static pressures, rocket-chamber pressure, base pressure, and pressure distribution over the port beach. The locations of the orifices for measuring base and beach pressures are shown in figure 5.

TEST PROCEDURES

The model and the booster assembly were launched from a mobile-type launcher inclined at an angle of approximately 60° above the horizontal as shown in figure 6. The model, which was accelerated to a maximum Mach number slightly greater than 1.5, separated from the booster assembly when the rocket motor in the model was ignited. The thrust of the rocket motor

contained in the model was such that the Mach number remained essentially constant during the time between booster separation and rocket-motor burnout. At the end of rocket burning it was intended that the model coast through the speed range, being decelerated by drag and the model weight component along the flight path.

During the flight of the model, information from each of the 14 instruments was transmitted from the telemeter in the model and received and recorded at the ground receiving station. At the ground station, a Doppler radar set and a radar tracking unit were used to determine the velocity of the model and its position in space. A radiosonde was used to measure atmospheric conditions at the time of flight.

RESULTS AND DISCUSSION

Visual observers on the ground reported that the model appeared to fly along a normal flight path during the time it was being accelerated by the booster assembly, but that soon after the model separated from the booster assembly it developed a noticeable lateral oscillation and then tumbled to the water. Tracking motion-picture-camera film showed that the vertical tail came off the model soon after the oscillation started. However, even though the model was in free flight for only a short time between separation from the booster, 3.3 seconds after take-off, and model failure, approximately 4 seconds after take-off, successful measurements were obtained through most of the interval that the scale rocket motors in the model were operating. Time histories of the basic quantities resulting from measurements made by the instruments in the model, the radar equipment at the ground station, and the radiosonde for the time interval between model separation from the booster and model failure are shown in figure 7.

Analysis of Model Lateral Instability

The variation of the side-force coefficient with time, shown in figure 7, shows a divergent lateral oscillation which indicates dynamic lateral instability. Even though the exact magnitude of the side-force coefficient at the time of model failure, approximately 4 seconds after take-off, cannot be determined because the range of the instrument was exceeded, the general character of the divergent lateral oscillation indicates that in all probability model failure was caused by excessive loads on the vertical tail.

A theoretical analysis of the dynamic lateral stability characteristics of an airplane requires that the inclination of the principal axis with respect to the body axis be known, but for this model the inclination

of the principal axis had not been determined. However, the probable inclination was estimated, from experience with similar models, to be within the limits of 1° and 7° nose down from the body axis. Accordingly, an analysis of the dynamic lateral stability characteristics was made by applying the stability derivatives presented in table II to the method of reference 1. The results obtained for the lateral oscillation mode are presented in figure 8 to show the variation of the amplitude ratio after one cycle with angle of attack for each of the two values describing the estimated limits of the inclination of the principal axis, $\epsilon = 1^{\circ}$ and $\epsilon = 7^{\circ}$. Thus, it can be seen in figure 8 that, for even the most favorable estimated inclination of the principal axis, $\epsilon = 1^{\circ}$, the calculations indicate that the model would have dynamic instability for negative angles of attack greater than -1.4°.

Even though the model tested had dynamic lateral instability under the test conditions, the full-scale airplane would probably be stable under sea-level conditions, as shown by the curve calculated by Convair in figure 8, because of the more favorable relative-density factor of the full-scale airplane (at sea level, approximately 1/6 that of the model, and as a result equal to the relative-density factor of the model at an altitude of about 47,000 feet).

Stability Parameters

Directional stability.- The directional-stability derivative C_{N_β} can be calculated from the time history of the side-force coefficient by the single-degree-of-freedom method which has been applied to another tailless airplane configuration in reference 2. Measuring the period of the oscillation and applying it and the necessary physical parameters of table I to the equation of reference 2 resulted in $C_{N_\beta} = 0.00023/\text{degree}$.

Longitudinal stability.- The values of C_N and α obtained during the time from 3.39 seconds to 3.44 seconds shown in figure 7 are plotted in figure 9 to show the variation of the normal-force coefficient with angle of attack. With the assumption that $C_N \approx C_L$, since the values of α are small, the experimental lift-curve slope obtained from figure 9 is approximately 0.03. This is considerably less than the value of approximately 0.04 obtained for the lift-curve slope during wind-tunnel tests of a nearly rigid model at $M = 1.5$ (ref. 3). The difference between the values of C_{L_α} obtained from this test and from the wind-tunnel tests is probably due in part to aeroelastic losses.

The variation of the angle of attack with time, shown at a large scale in figure 10, and the slope of the lift curve obtained from figure 9 were used in conjunction with the methods included in reference 4 to determine C_{m_α}, $C_{m_q} + C_{m_{\dot{\alpha}}}$, and C_m/C_L. [redacted]

The pitching-moment coefficient at zero lift was estimated from the equation

$$C_{m_o} = -C_{m_\alpha}\left(\alpha_t - \alpha_o\right) - C_T \frac{z}{\bar{c}}$$

The value of α_o, while not being accurately known, can be determined from figure 9 to fall between 0° and 0.3°. Therefore, since $\alpha_t \approx -2.1^\circ$, neglecting α_o results in an error in the first term no greater than 15 percent. Thus, neglecting α_o, $C_{m_o} = -0.10$.

The model stability characteristics as determined from this test are compared in the following table with stability characteristics obtained under nearly rigid conditions from wind-tunnel tests at $M = 1.5$:

	0.10-scale rocket model	0.017-scale wind-tunnel model (ref. 3)
Center-of-gravity position, percent M.A.C.	29.7	30.0
C_{m_α}/deg	-0.0059	-0.0073
C_{m_o}	-0.010	-0.007
C_m/C_L from L.E. of M.A.C.	-0.49	-0.48
$\left(C_{m_q} + C_{m_{\dot{\alpha}}}\right)$/rad	-0.70	-------
C_{n_β}/deg	0.00023	0.00109

Differences between rocket model and wind-tunnel results are greatest for C_{m_α}, C_{n_β}, and C_{m_o}, which is discussed in the next section. The difference in C_{m_α} is due to the difference in C_{L_α} previously noted. The disagreement in the value of C_{n_β} is probably due to model flexibility since the value of C_{n_β} estimated by Convair for the full-scale flexible airplane at sea level at $M = 1.5$ and listed in table II is 0.00024/deg which is very close to the value obtained in this test. The value of $C_{m_q} + C_{m_{\dot{\alpha}}}$ while obtained during power-on flight represents the power-off case, since the rocket thrust and angles of attack were small. The value agrees with the results of reference 5 which were obtained for a thin, aspect-ratio-2, delta wing and body.

Lift, Pitching Moment, and Drag Contributed by the Beach

The pressures measured on the beach area, at the locations shown in figure 5, are probably indicative of those on the full-scale airplane because of the close similarity between the rocket engine and the turbojet-engine characteristics as shown in the following table. (Characteristics of the rocket motor used in the 1/10-scale model were obtained from static ground tests):

	1/10-scale rocket model (average values)	Full-scale airplane (M = 1.5; altitude, 35,000 ft; afterburner on)
$\frac{\text{Exit weight flow}}{\text{Theoretical inlet weight flow}}$ . . .	0.84	0.78
$\frac{\text{Exit total pressure}}{\text{Stream static pressure}}$	7.59	7.83
$\frac{\text{Exit static pressure}}{\text{Stream static pressure}}$	4.25	4.31
C_T	0.041	0.036
Exit area, sq in.	2.85	285
Exit Mach number	1.0	1.0

The time histories of the pressure coefficients, presented in figure 7, indicate pressures considerably less than atmospheric over the beach, during power-on flight. Since no power-off data were obtained, the effect of the jet on the pressure on the beach cannot be determined. In order to estimate the effect of the pressure on the beach during power-on flight on the model aerodynamic characteristics, it has been assumed that the pressures measured on the beach along the jet center line are representative of the pressures around the beach. While the pressure measurements at station 56.25 indicate that the assumption is not strictly correct, the assumption will give conservative results. The variation of the pressure coefficient has been assumed to be linear along the beach surface between the stations where the pressure measurements were made (fig. 11(a)). Also, as shown in figure 11(a), the pressure coefficient was assumed to remain constant aft of the last pressure orifice; however, this assumption will not lead to large errors since the effective area on which the beach pressures act decreases rapidly near the rear of the beach (fig. 11(b)). The product of the normal component of the pressure coefficient and the effective area K is shown in figure 11(c) as F_n. The lift coefficient calculated from

$$C_{L_{beach}} = \frac{2}{144S}\int_{\text{Station } 54.25}^{\text{Station } 62.5} F_n \, dx$$

was found to be equal to -0.0056 (total for both beach areas). Similarly, the moment coefficient was -0.0044. Thus it appears that the difference in the C_{m_0} values obtained from the present test and from wind-tunnel tests can be accounted for by the pressures over the beach. For the wind-tunnel tests of reference 3, the aft portion of the model, including the beach area, was modified to incorporate the model support system, and thus the results included no beach effects. The drag coefficient contributed by the beach area was calculated to be 0.002.

Drag

The drag coefficient and the lift coefficient were calculated in the time interval from 3.38 seconds to 3.45 seconds, by the equations

$$C_D = \frac{C_N\alpha}{57.3} - C_C + C_T$$

and

$$C_L = C_N$$

To extend the range of values as much as possible, C_D and C_L were also calculated during the time that the C_N instrument was against the stop by applying the product of C_{N_α}, obtained from figure 9, and the appropriate angle of attack from figure 10 in place of experimental values of C_N in the same equations used previously. These calculated values, as shown in figure 12, cover only a small part of the range needed to establish a drag polar; however, by comparing these values with a drag polar obtained for a 0.017-scale model at $M = 1.5$ in a wind-tunnel test (ref. 3) and assuming that $C_{D_{min}}$ would occur at the same C_L for both tests, it is possible to estimate $C_{D_{min}}$ for this test as approximately 0.035 as compared with 0.028 obtained in the wind-tunnel test. The drag of the wind-tunnel model is probably low since the aft portion of the fuselage differed from the airplane. The drag of the rocket model is probably greater than that of the airplane because of the blunt inlet-duct fairings which would correspond to low inlet mass flow. The rocket base annuli contributed approximately 0.0015 to the model drag coefficient.

CONCLUSIONS

The results of the power-on flight at $M = 1.53$ of a 1/10-scale model of the Convair XF2Y-1 airplane containing solid-fuel rocket motors

designed to simulate full-scale turbojet-engine characteristics with full afterburning at an altitude of 35,000 feet indicate the following conclusions:

1. The model had dynamic lateral instability, but under conditions not likely to be encountered by the full-scale airplane.

2. The value obtained for the pitching moment at zero lift was approximately 30 percent greater (nose down) than the value obtained from wind-tunnel tests; however, this difference was accounted for by calculation of the pitching moment contributed by the low-pressure regions over the beach areas.

3. The value obtained for the directional-stability parameter, while differing widely from the results of wind-tunnel tests (probably because of model flexibility), agreed very well with the value estimated by Convair for the full-scale flexible airplane at sea level.

4. Compared with wind-tunnel results, the value of 0.03 obtained for the lift-curve slope during this test was approximately 25 percent low. The difference is probably due in part to wing aeroelastic losses.

5. The extrapolated minimum drag coefficient obtained for this model, which had inlets that were faired with approximately spherical covers, was approximately 25 percent higher than the drag obtained from wind-tunnel tests of a model with open inlets, but having a different aft fuselage geometry.

Langley Aeronautical Laboratory,
National Advisory Committee for Aeronautics,
Langley Field, Va., September 15, 1953.

William M. Bland, Jr.
Aeronautical Research Scientist

Robert L. Nelson
Aeronautical Research Scientist

Approved: Joseph A. Shortal
Joseph A. Shortal
Chief of Pilotless Aircraft Research Division

mhg

[redacted]

REFERENCES

1. Campbell, John P., and McKinney, Marion O.: Summary of Methods for Calculating Dynamic Lateral Stability and Response and for Estimating Lateral Stability Derivatives. NACA Rep. 1098, 1952. (Supersedes TN 2409.)

2. Purser, Paul E. and Mitchell, Jesse L.: Miscellaneous Directional-Stability Data for Several Airplane-Like Configurations From Rocket-Model Tests at Transonic Speeds. NACA RM L52E06b, 1952.

3. Strayer, R. E.: XF2Y-1 Airplane Configuration – Fourth Supersonic Test at M = 1.50 at OAL, Daingerfield, Texas: OAL Test 233-7. Memo A-2-7, Consolidated Vultee Aircraft Corp., Jan. 15, 1952.

4. Gillis, Clarence L., Peck, Robert F., and Vitale, A. James: Preliminary Results From a Free-Flight Investigation at Transonic and Supersonic Speeds of the Longitudinal Stability and Control Characteristics of an Airplane Configuration With a Thin Straight Wing of Aspect Ratio 3. NACA RM L9K25a, 1950.

5. Tobak, Murray: Damping in Pitch of Low-Aspect Ratio Wings at Subsonic and Supersonic Speeds. NACA RM A52L04a, 1953.

6. Frick, J., Thomas, D., Meyer, R., and Janowitz, W.: Stability and Control Summary Report of the Revised Y2-2 Airplane. Rep. No. ZA-2-003 (Contract N0a(S)-10507 Amendment #4), Consolidated Vultee Aircraft Corp., May 14, 1951.

TABLE I

GENERAL CHARACTERISTICS OF MODEL

Wing:	
Total included area, sq ft	5.63
Span, ft	3.37
Mean aerodynamic chord, ft	2.14
Aspect ratio	2.03
Airfoil section:	
At center line	NACA 0002.89-65 (modified)
From 86 percent of half-span to tip	NACA 0004-65 (modified)
Tail:	
Exposed area, sq ft	0.80
Airfoil section:	
At root	NACA 0003-65 (modified)
At tip	NACA 0004-65 (modified)
Elevon deflection, deg	0
Weight*, lb	94.16
Moment of inertia about body axes*, slug-ft^2:	
Roll	0.51
Yaw	5.17
Pitch	4.58
Center-of-gravity position*:	
Percent $\bar{c}$	29.7
In. above reference line	0.8

*Average values during test.

[redacted]

TABLE II

STABILITY DERIVATIVES USED IN DYNAMIC-LATERAL-STABILITY ANALYSIS

[Derivatives estimated by Convair for the full-scale flexible airplane at $M = 1.5$ at sea level, except where noted]

$C_{l_p} = -0.00227/\text{deg}$	$C_{n_p} = 0.00018/\text{deg}$	$C_{Y_p} = -0.00175/\text{deg}$
$C_{l_r} = 0.00087/\text{deg}$	$C_{n_r} = -0.00087/\text{deg}$	$C_{Y_r} = 0/\text{deg}$
$C_{l_\beta} = -0.00027/\text{deg}^{**}$	$C_{n_\beta} = 0.00023/\text{deg}^{*}$	$C_{Y_\beta} = -0.00900/\text{deg}$

*The value of C_{n_β} estimated by Convair, 0.00024, was replaced by the experimental value.

**The value of C_{l_β} estimated by Convair, -0.00035, was replaced by the value in the table to serve as an adjustment for the trim angle of attack as indicated by wind-tunnel results of ref. 6.

DE[redacted]SIFIED

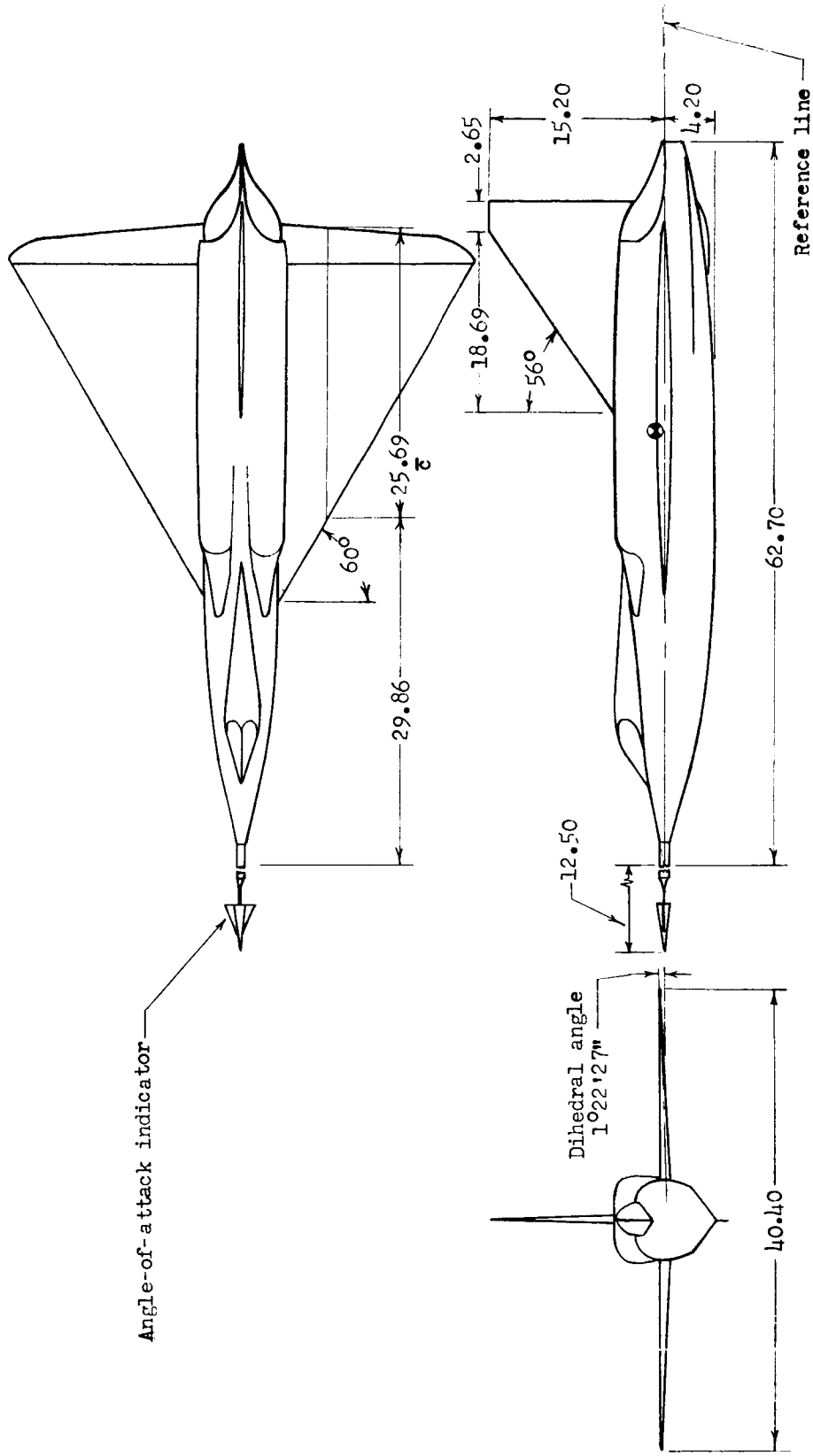

Figure 1.- General arrangement of model. All linear dimensions in inches.

[redacted]

[redacted]

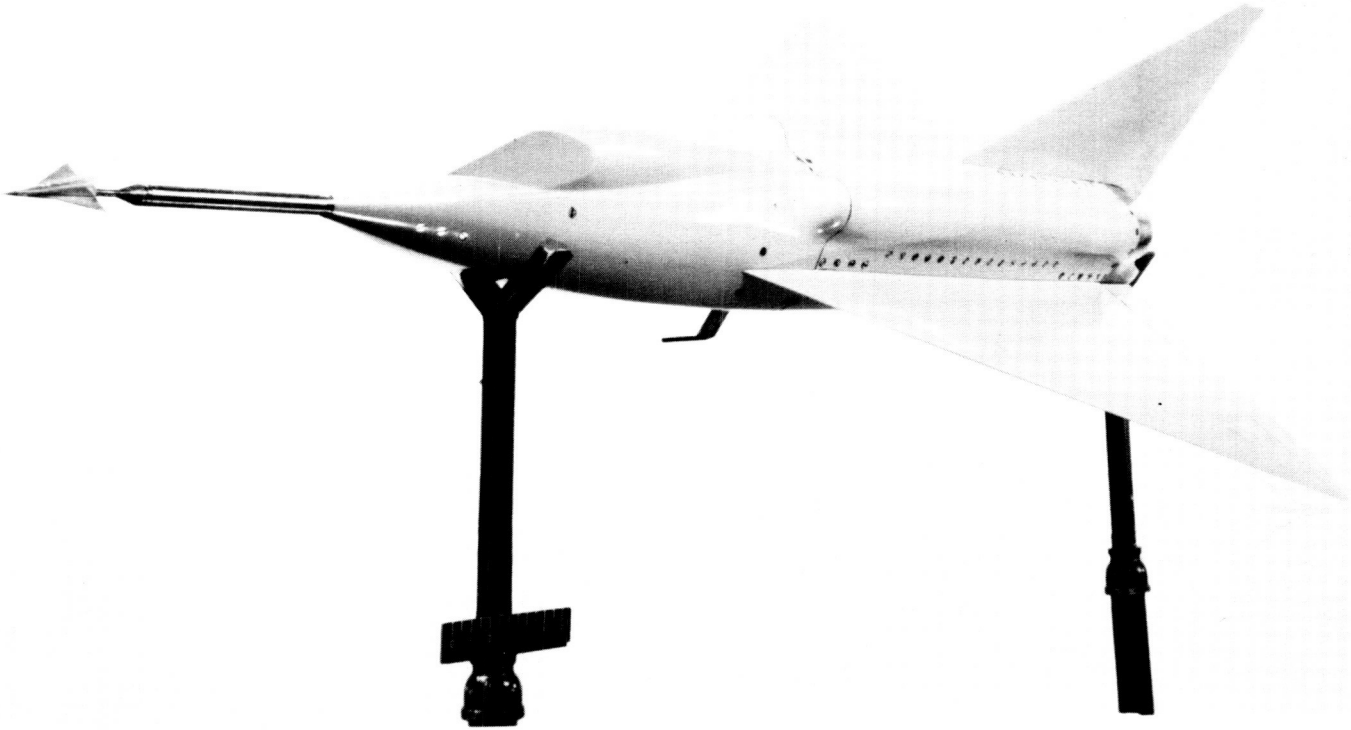

L-77630.2

(a) Three-quarter front view.

Figure 2.- External views of model.

[redacted]

DECL[redacted]IFIED

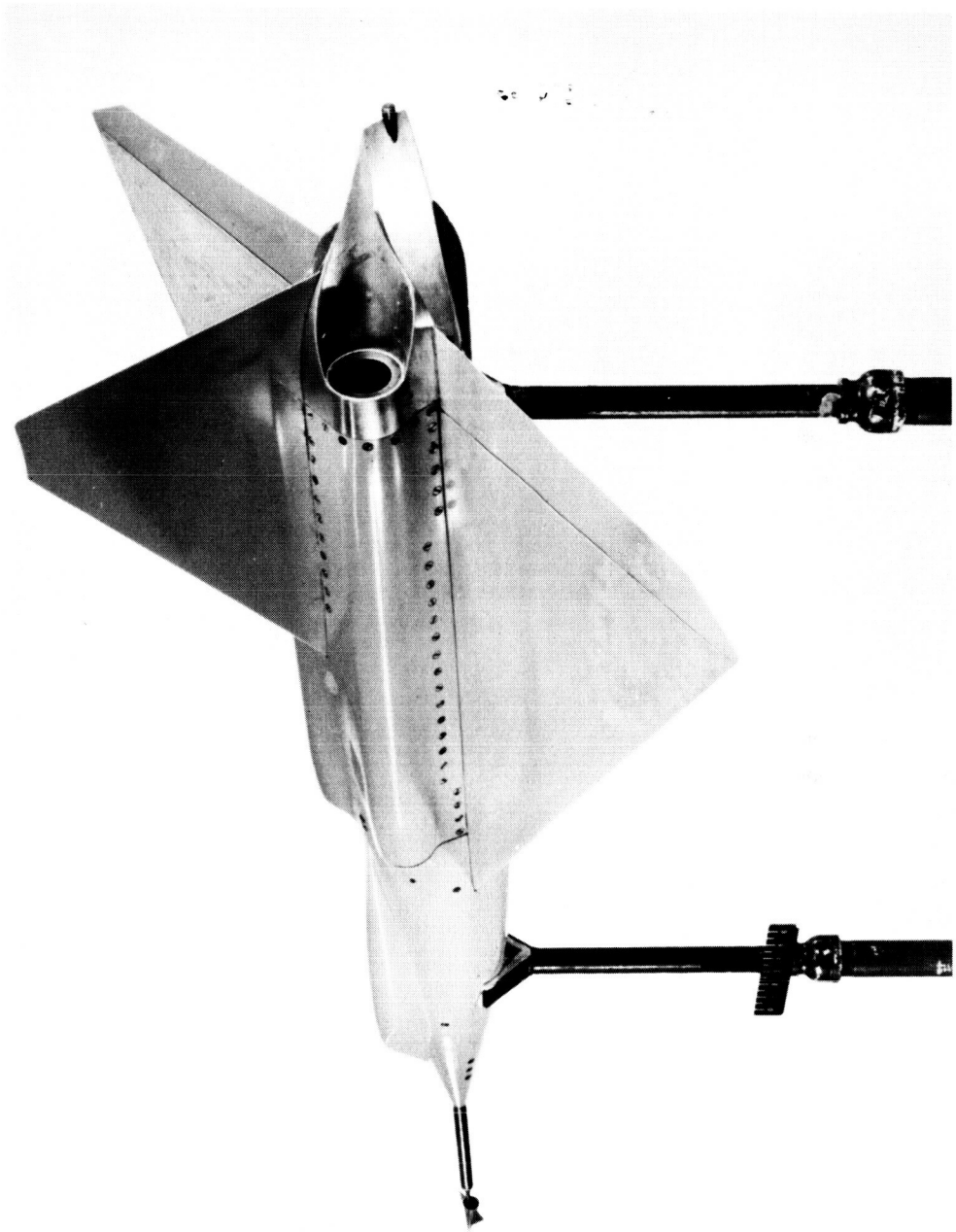

L-77631.1

(b) Three-quarter rear view.

Figure 2.- Concluded.

[redacted]

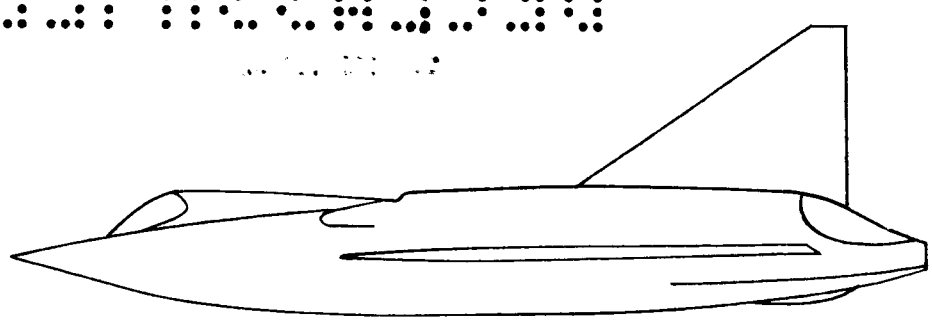

Model

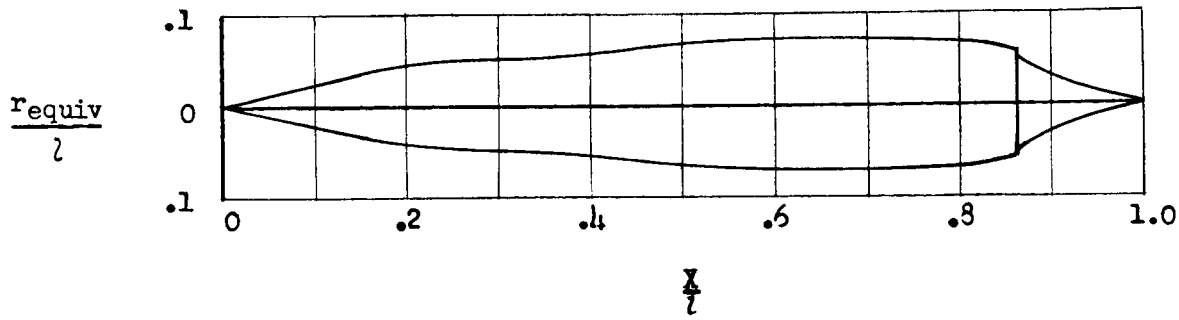

Equivalent body, $\frac{l}{D_{max}} = 6.98$

$l = 62.7$ inches for 1/10-scale model

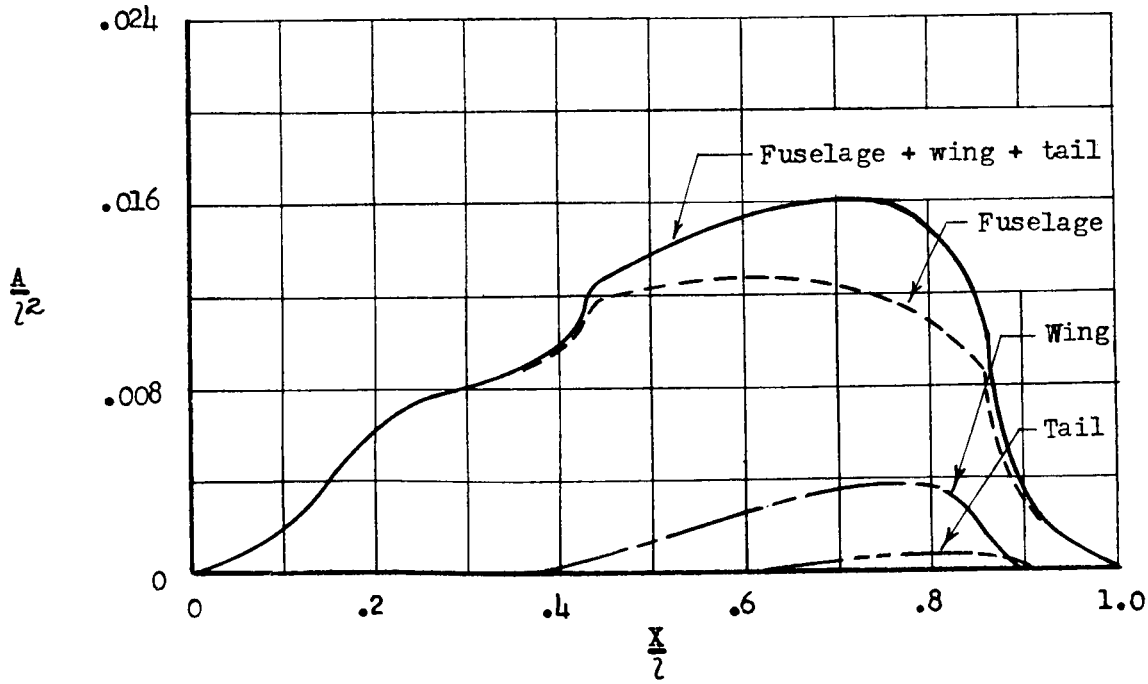

Figure 3.- Area distribution of model including area of closed ducts and profile of body of revolution with equivalent area distribution.

[redacted]

 DECL[redacted]IFIED

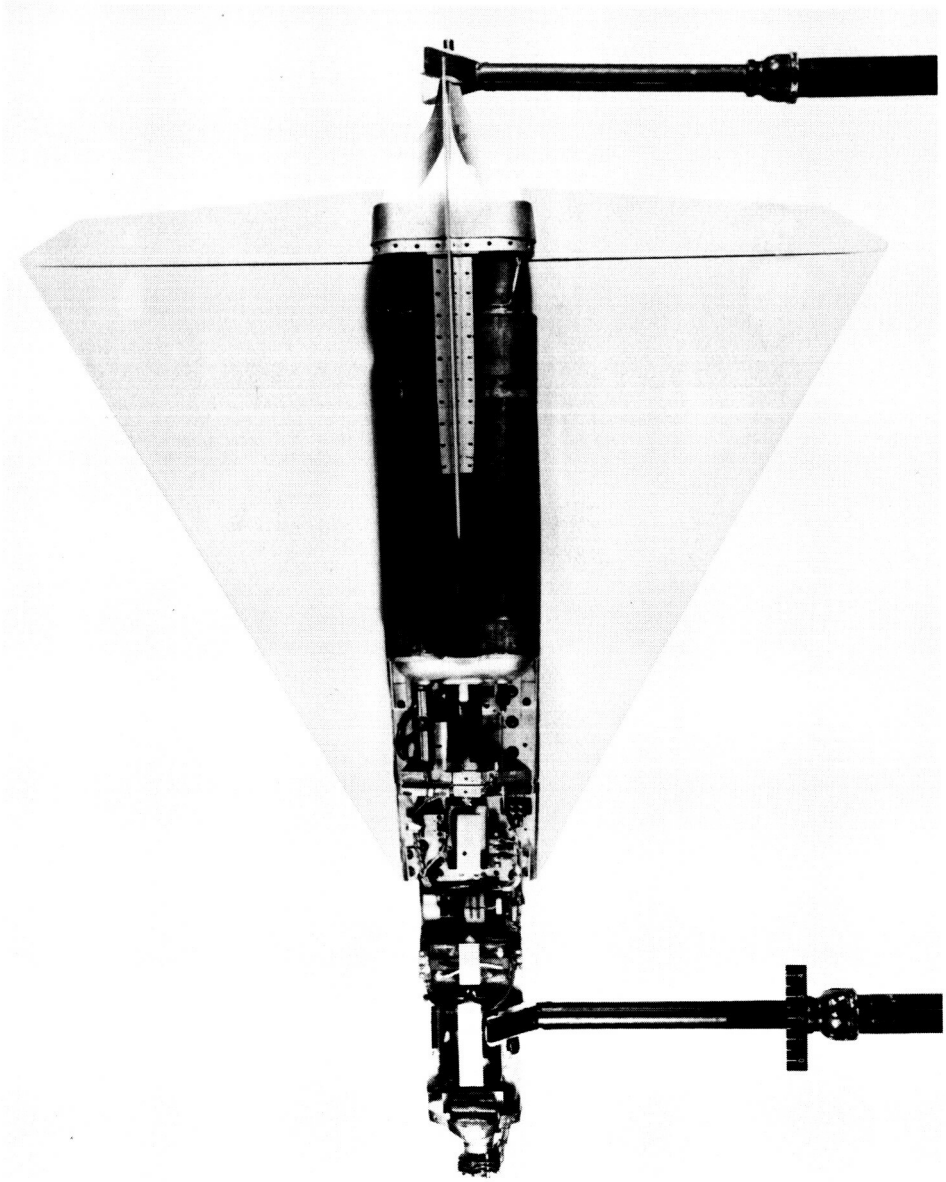

L-77634.1

(a) Nose and top cover removed to show some instrumentation and the rocket-motor installation.

Figure 4.- Internal details of model.

[redacted]

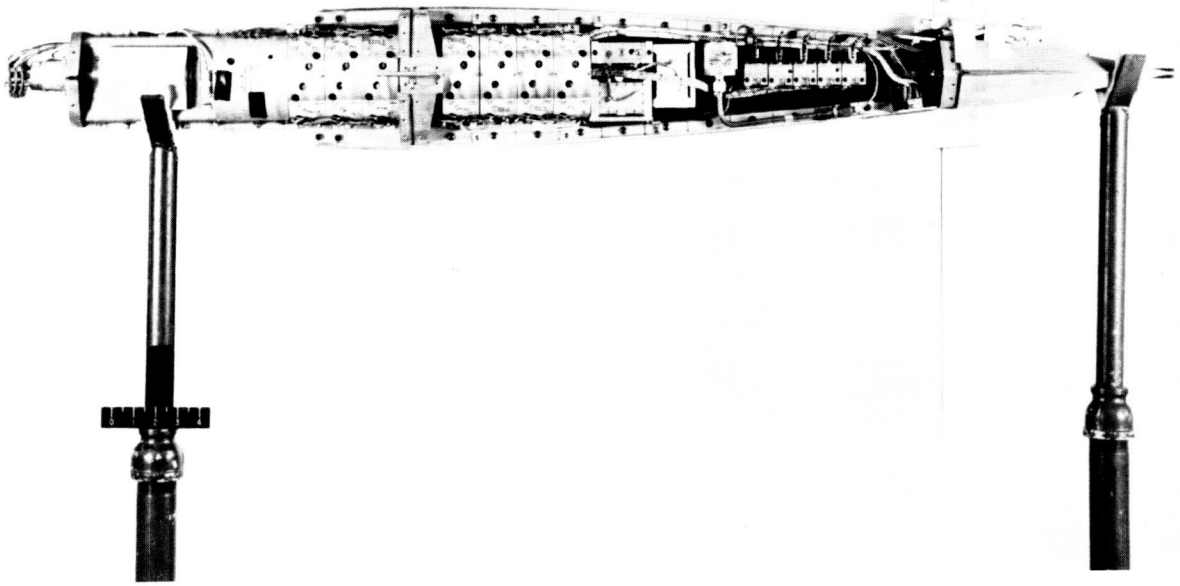

L-77632.1

(b) Nose and bottom cover removed to show telemeter and other instrumentation.

Figure 4.- Concluded.

 DECL[redacted]L

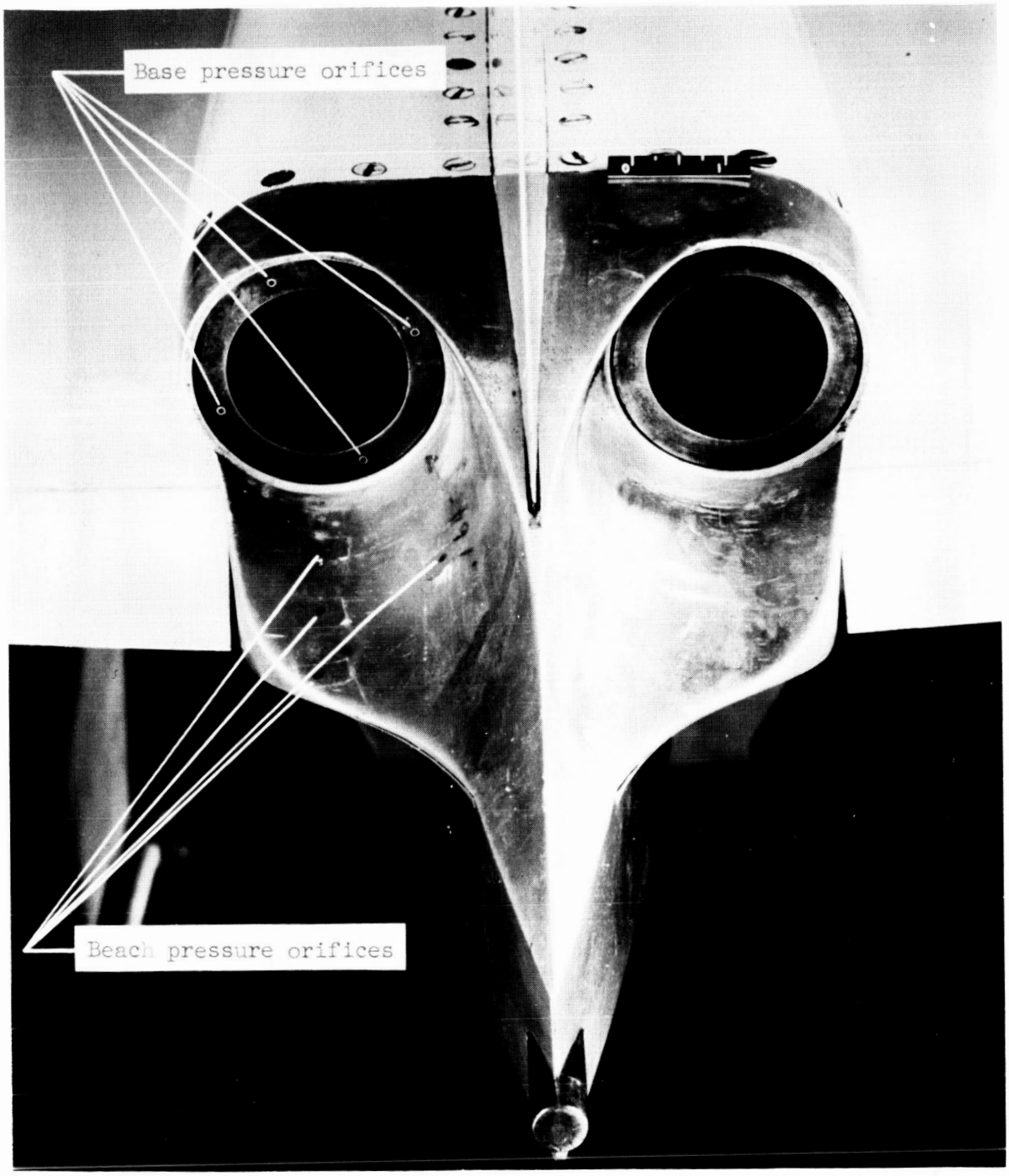

L-77636.1

(a) Photograph of aft end of model.

Figure 5.- Locations of beach pressure orifices and base pressure orifices.

[redacted]

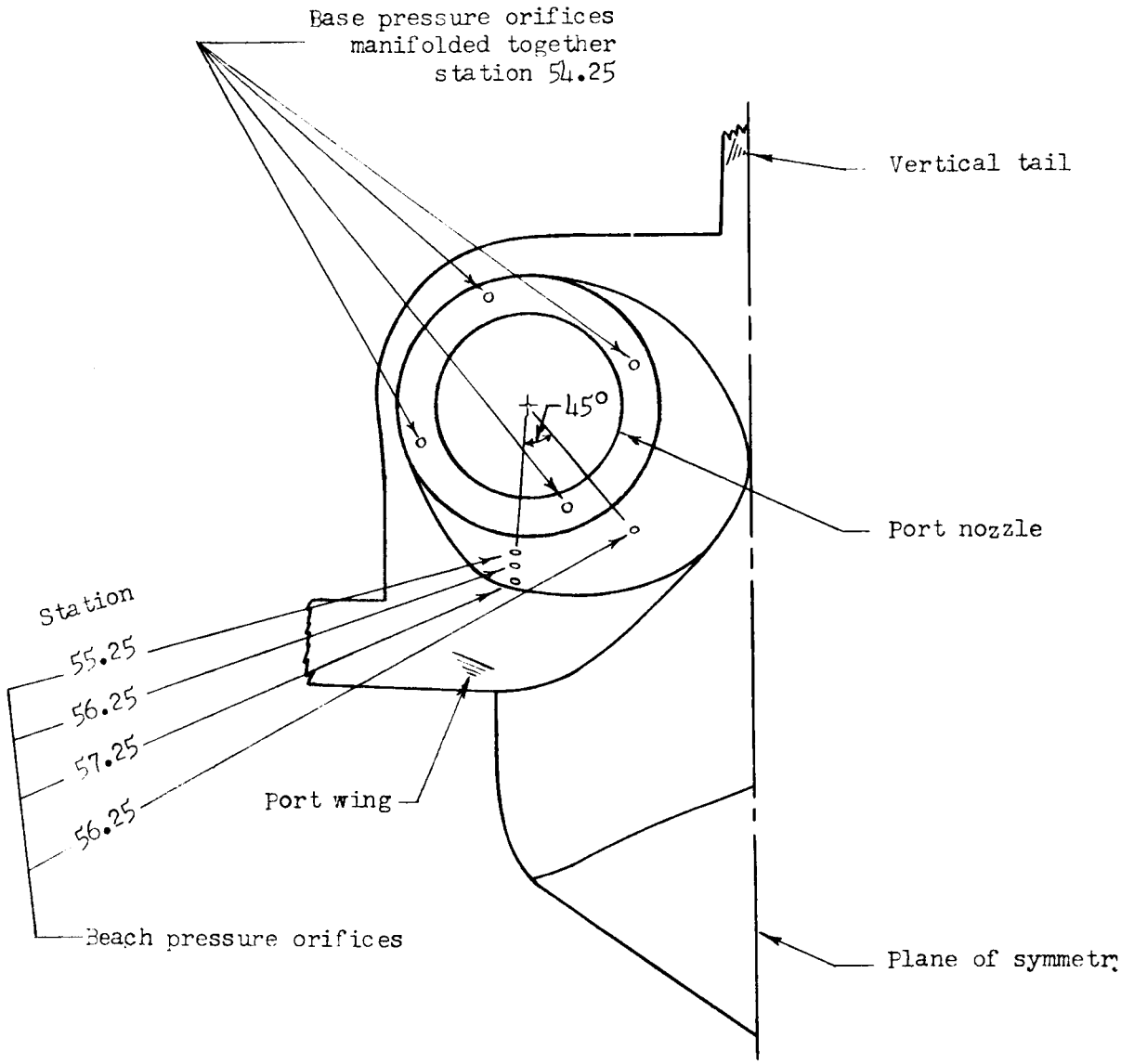

(b) Sketch of a portion of aft end of model, looking forward.

Figure 5.- Concluded.

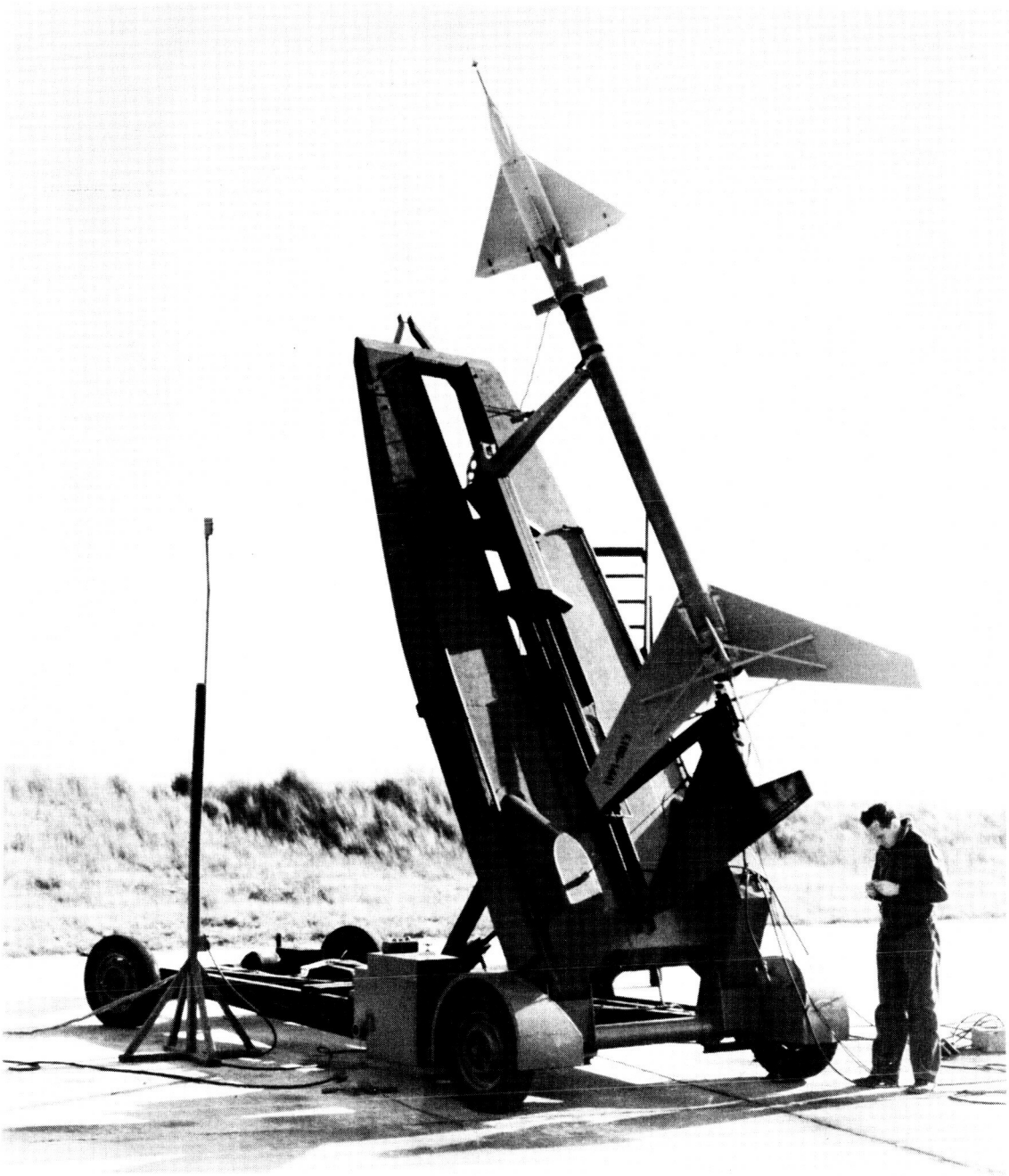

L-78048

Figure 6.- Model and booster assembly on the launcher.

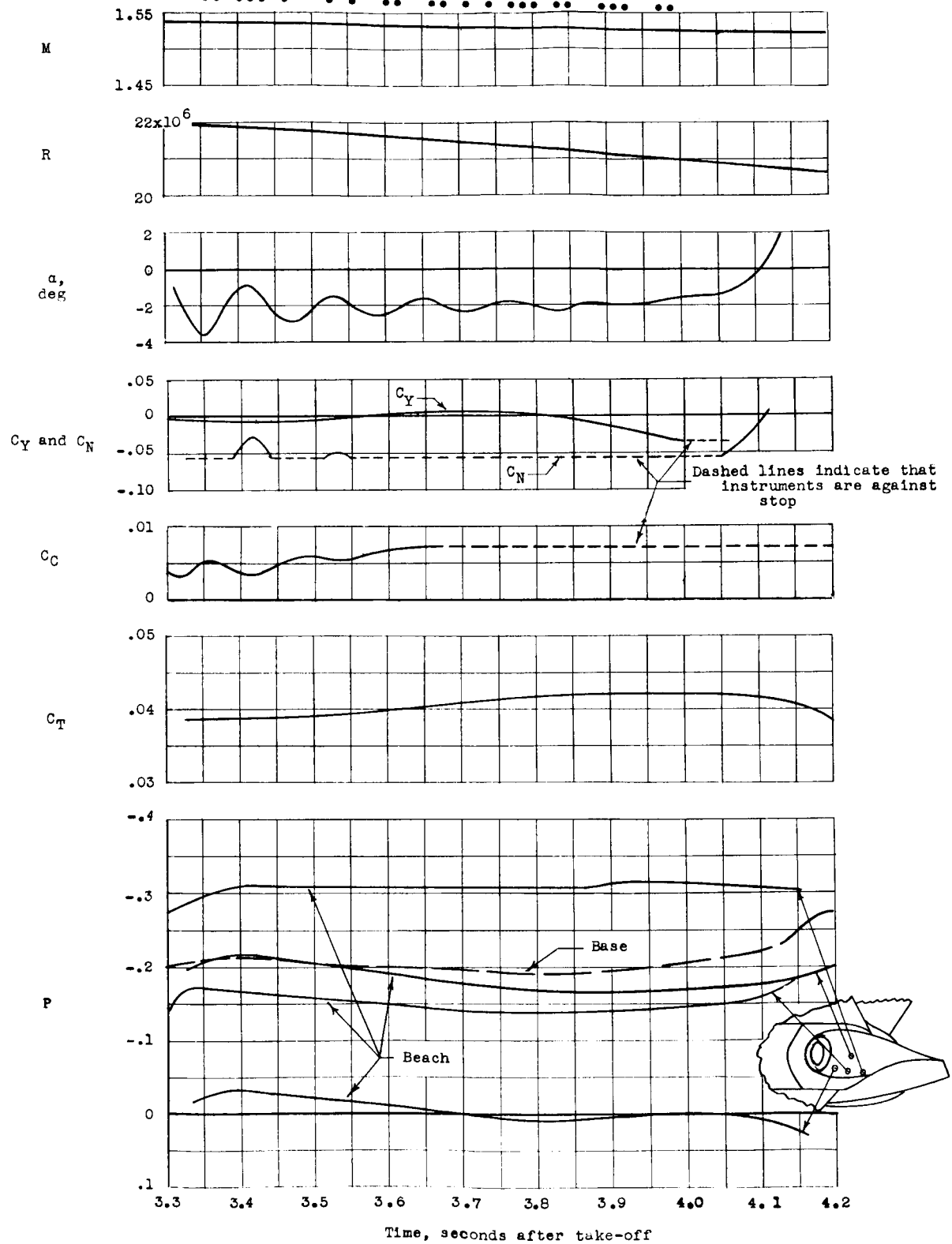

Figure 7.- Time histories of the quantities measured during model flight after separation from the booster.

[redacted]

 DECLASSIFIED

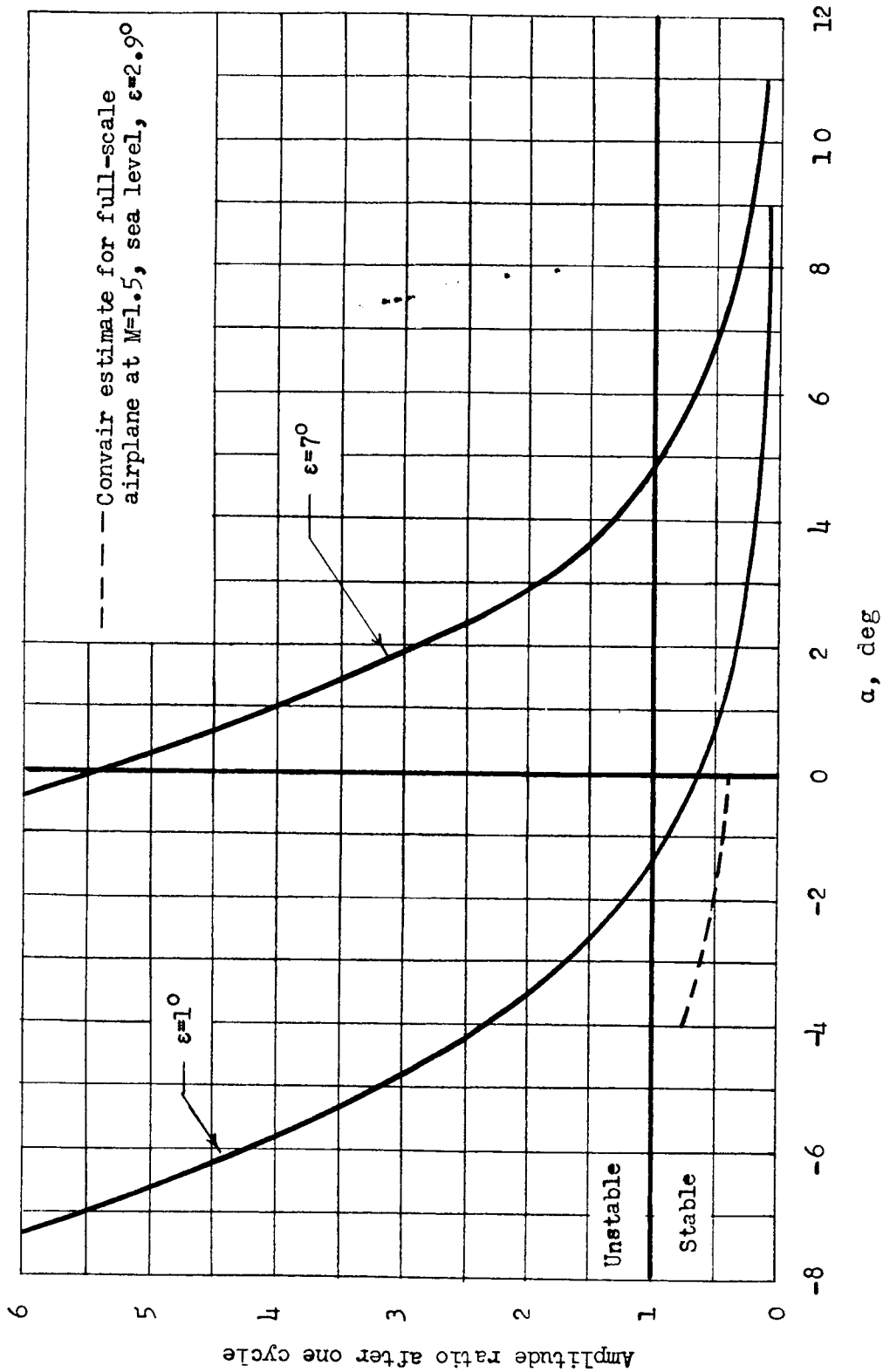

Figure 8.- The amplitude ratio after one cycle of the lateral oscillation as a function of the angle of attack as calculated using the stability derivatives in table II and the method of reference 1.

[redacted]

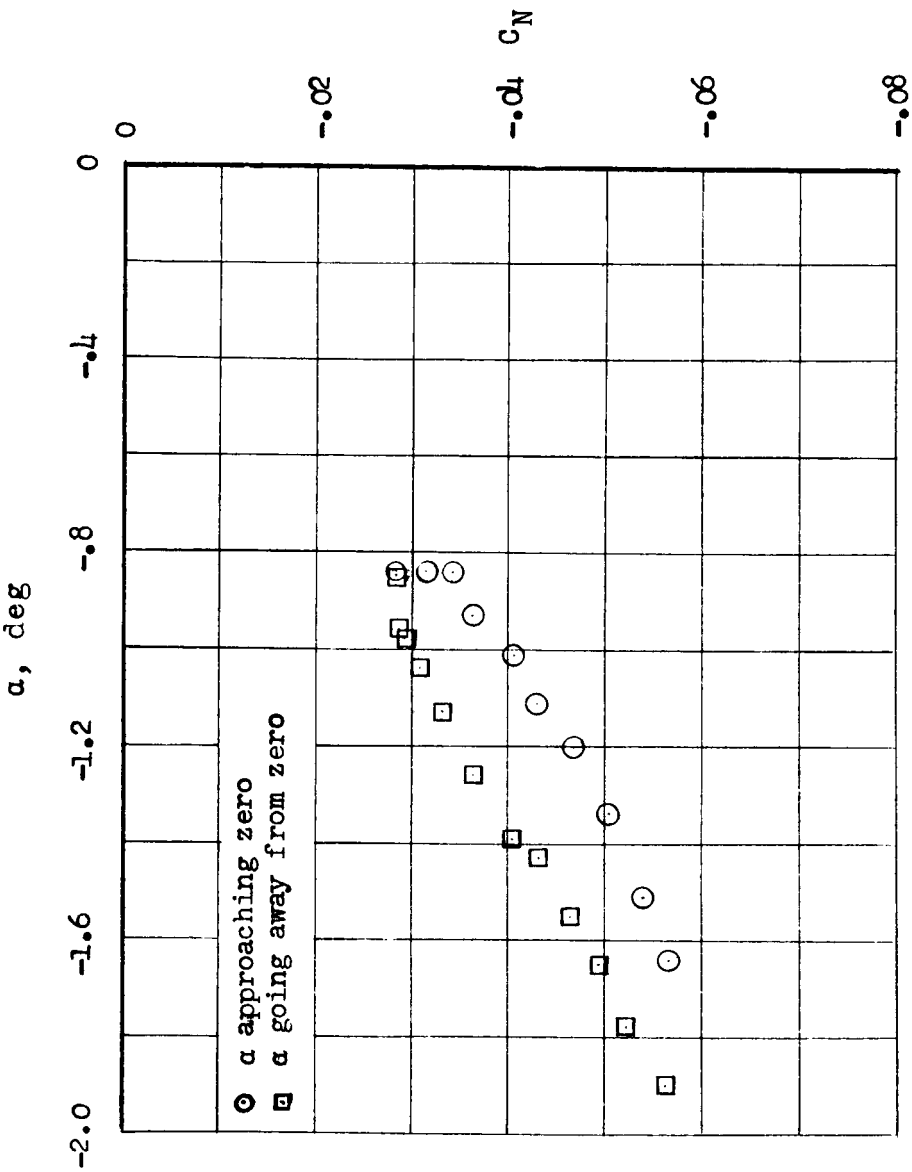

Figure 9.- The variation of the normal-force coefficient with angle of attack.

[redacted]

 DECL[redacted]ED

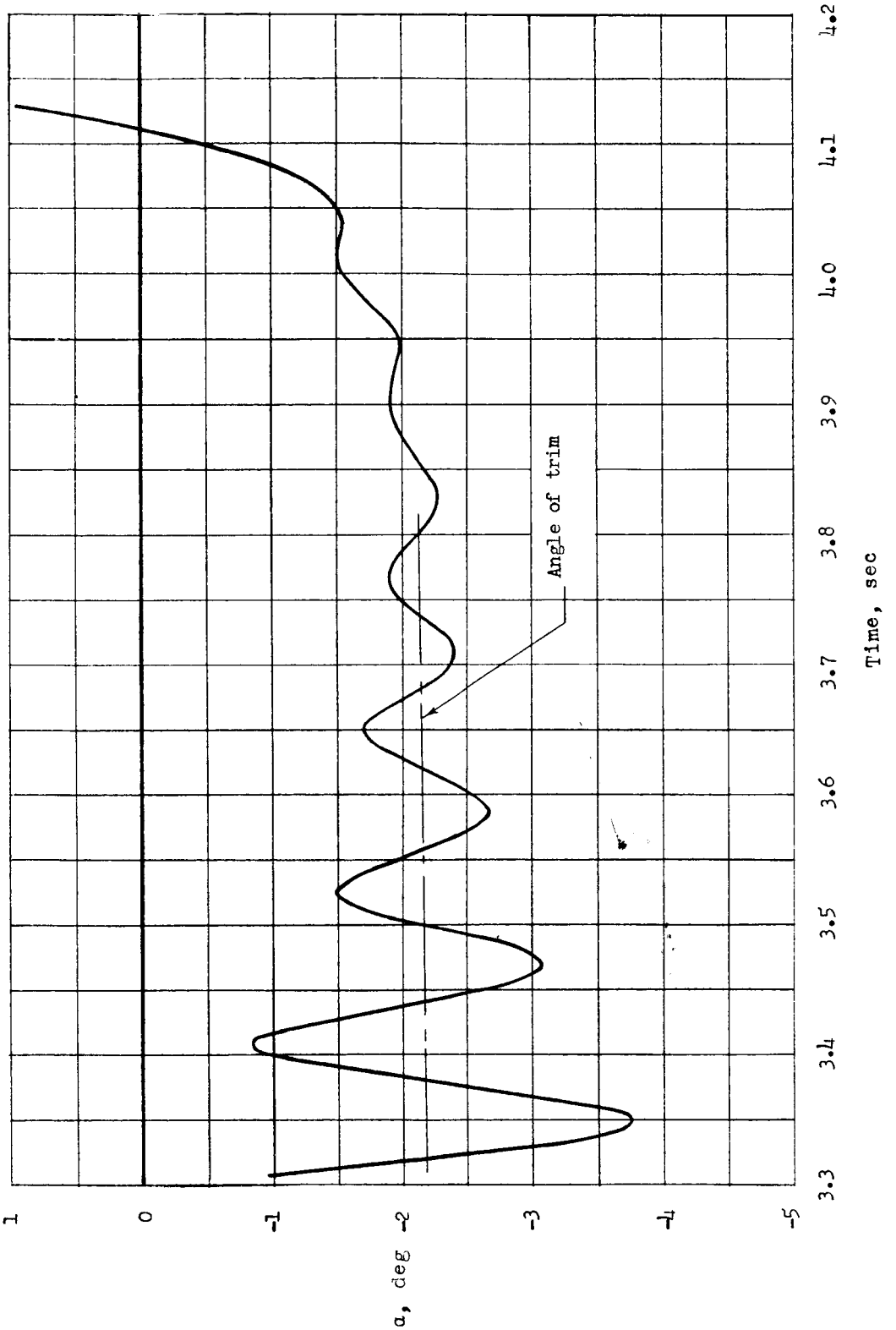

Figure 10.- The variation of angle of attack with time.

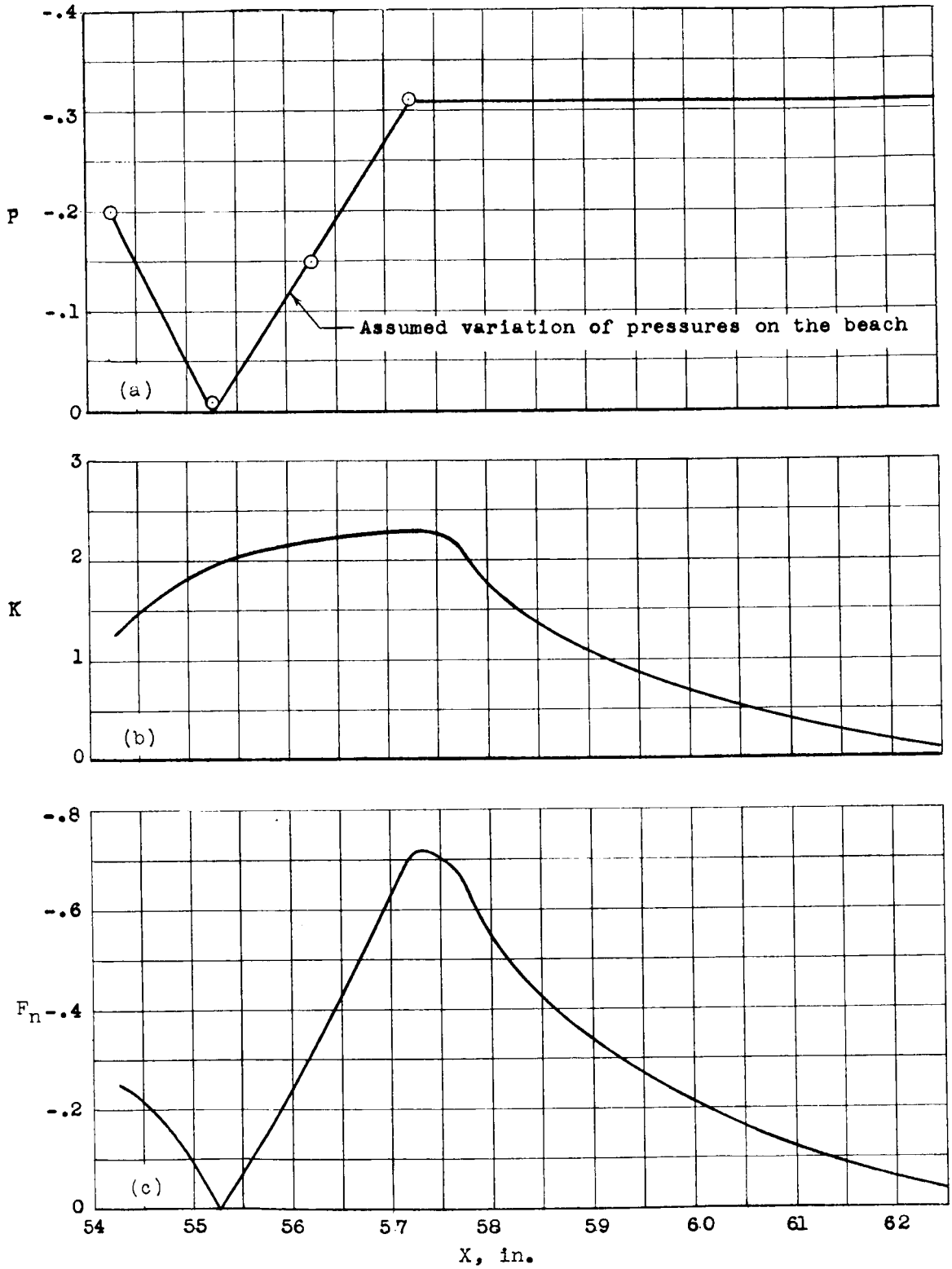

Figure 11.- Estimation of the effect of pressures over the beach on the model pitching moment.

[redacted]

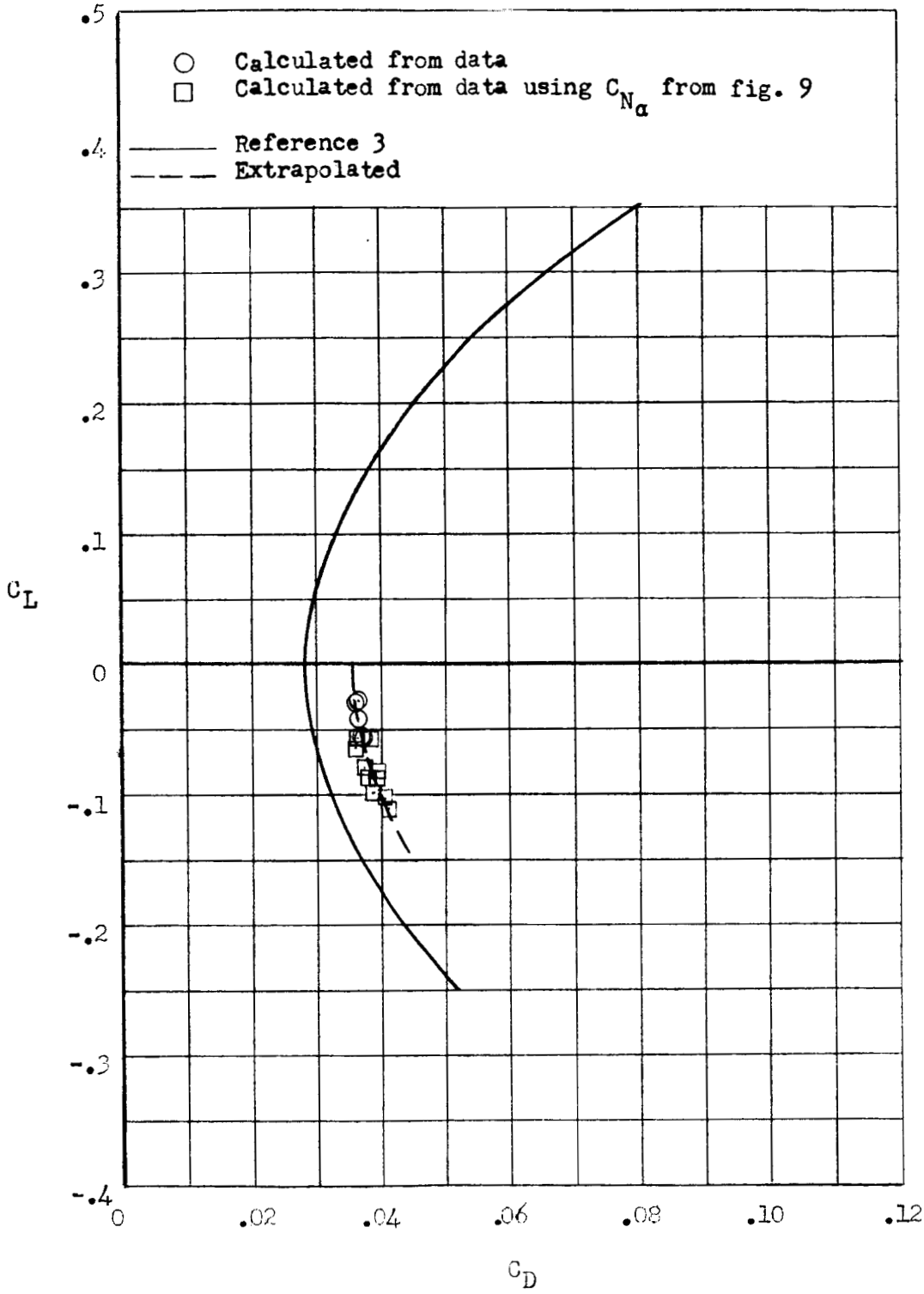

Figure 12. The variation of drag coefficient with lift coefficient.